J. Chem. Phys., accepted (Nov. 2007)

PREPRINT

Field Response and Switching Times in Biaxial Nematics

Roberto Berardi*, Luca Muccioli, and Claudio Zannoni,

Dipartimento di Chimica Fisica e Inorganica, and INSTM-CRIMSON,

Università di Bologna,

Viale Risorgimento 4, 40136 Bologna, Italy

Monday, October 22, 2007

Abstract

We study by means of virtual molecular dynamics computer experiments the response of a bulk biaxial nematic to an applied external field and in particular the relative speed of reorientation of the principal director axis and of the secondary one, typical of these new materials, upon a $\pi/2$ field switch. We perform the simulations setting up and integrating the equations of motion for biaxial Gay–Berne particles using quaternions and a suitable time reversible symplectic integrator. We find that switching of the secondary axis is up to an order of magnitude faster than that of the principal axis, and that under fields above a certain strength a reorganization of local domains, temporarily disrupting the nematic and biaxial ordering, rather than a collective concerted reorientation occurs.

KEYWORDS: biaxial nematics, liquid crystals, molecular dynamics, Gay–Berne potential, quaternions, symplectic integrator, angular momentum, director dynamics.

1 Introduction

The discovery of biaxial nematic (BXN) materials,[1–5] after their existence had been long theoretically predicted[6] and confirmed by computer simulations,[7,8] has opened new potential developments for fast responding and possibly bistable displays. The essence behind these expectations is the existence of two preferred directions, i.e. of a secondary axis director in addition to the principal axis one characteristic of ordinary nematics. The flourishing of activities involving BXN comprises spectroscopical characterization by NMR,[1] X–ray,[2] dichroic[3] and light scattering[9] methods, as well as computer simulations,[10,11] and theory.[12]

Computer simulations are of particular importance in these complex systems also from the point of view of investigating their potential applications in view of the difficulty, at least for the time being, of deploying BXN materials with existence temperature, viscosities and elastic constants all falling in a range convenient for electro–optic applications (not to mention the design of a suitable switching cell). Theoretical investigations are also far from simple. For instance, the number of elastic constants for a BXN are over a dozen[13–15] and a similar proliferation of specific material constants occurs for other properties, e.g. rheological.[16,17] Apart from widening the gap between molecular and material properties, this causes obvious computational difficulties in setting up, parameterizing and solving even simple models for studying the response of a BXN to an external field.[18] Here we wish to tackle this problem, central to the use of BXN in electro–optical devices, by using molecular resolution off–lattice simulations.[19] In particular, we are interested in estimating the relative response times of bulk BXN directors to a switching field applied in different directions. This seems particularly timely in view of recent experimental measurements, on a bent–core BXN[20] in a planar confined geometry, where the expected faster switching driving the secondary director of BXN with respect to the usual principal anisotropy axis was actually observed. To study the response we resort to our previous modelling of BXN in terms of a biaxial

attractive–repulsive (Gay–Berne type[21]) potential.[10,19,22] We have in fact shown that by suitably parameterizing the biaxiality of the attractive and repulsive parts of the potential, a stable thermotropic BXN phase can be obtained. Monte Carlo (MC)[23,24] simulations showed this phase to be an orthogonal nematic biaxial phase intervening between a uniaxial nematic (at higher temperature), and a biaxial smectic (at lower temperature). Starting from BXN samples obtained with this parameterization, we can study the behavior of the principal and secondary directors of the bulk fluid when an external field is applied or switched off. To follow its relaxation time we employ molecular dynamics (MD)[23,24] simulations with a purpose written code implementing torque and orientational evolution integrator[25] based on quaternions.[26] In the next section we describe our model and virtual experiments in detail, while in later ones we present and discuss the simulation results.

2 Model

We wish to consider a fluid system of rigid biaxial particles subjected to an external field, applied along a certain direction, that can be switched to another one of choice so as to measure the time required by the nematic sample to adjust to the new field direction (see Figure 1). The total energy of our model is the sum of two contributions: a potential term which accounts for the short–range dispersive interactions between all pairs of particles with distance smaller or equal than a cutoff radius, and a field term which gives the total interaction between the particles and the external switching field.

2.1 Potential, force and torque in a systems of biaxial GB particles

In our previous work on the modelling of biaxial mesogens at molecular resolution level[22,27] we have already developed a biaxial extension of the Gay–Berne (GB) potential,[21] an off-lattice model which has been successfully used for the computer simulation

of mesogenic systems.[19,28,29] We have also shown[10] that stable thermotropic BXN, as needed for our proposed switching experiment, can be obtained with an appropriate parameterization of such potential. However, until now, we have essentially studied static equilibrium properties using MC simulations.[10] Since here we need instead to study time evolutions, the use of the molecular dynamics (MD) [23,24] technique is more appropriate. In order to implement MD we have to set up and integrate the equations of rotational motion for a system of rigid biaxial particles in a form that is free from spurious singularities and a quaternion representation[30] is particularly suitable for this purpose. More specifically this means to derive expressions for the computation of the torque acting on each biaxial molecule because of its interactions with the other particles as well as with the external field. Here we start reformulating the biaxial GB potential in terms of quaternions and proceed deriving explicitly the required derivatives. To keep the treatment as self–contained as possible we report in the Appendix some of the necessary background material in terms of quaternions and integrators. We notice that the translational motion is not an issue here since it is described by standard equations.[23,24,31]

2.2 Biaxial Gay–Berne potential

The biaxial extension of the Gay–Berne potential[21,22,27] (BXGB) describes the anisotropic interaction between a pair of rigid ellipsoidal particles, and it is parameterized in terms of their axes lengths σ_x, σ_y and σ_z, their potential well depths ϵ_x, ϵ_y and ϵ_z and, further, by two additional parameters μ and ν that tune the shape of the potential.[10,22,27] An additional quantity, σ_c the so–called *"minimum contact distance"*, determines the energy wells width. The most general form of this potential can model the heterogeneous interaction between dissimilar ellipsoids.[27] Anyway, since this paper considers a single–component system we will omit from the equations the superscripts labelling the various species. More explicitly, the potential between a pair of biaxial molecules α and β can be written as[22,27]

$$U(\mathbf{r},\mathbf{Q}) = 4\epsilon_0\,\epsilon(\mathbf{r},\mathbf{Q})\left[u^{12}(\mathbf{r},\mathbf{Q}) - u^{6}(\mathbf{r},\mathbf{Q})\right], \tag{1}$$

where $u(\mathbf{r},\mathbf{Q}) \equiv \sigma_c/(r-\sigma(\mathbf{r},\mathbf{Q})+\sigma_c)$, and ϵ_0 defines the energy scale. We use the symbol $\mathbf{Q}$ as a shorthand for the two quaternion operators $[\mathbf{q}^\alpha\rangle$, and $[\mathbf{q}^\beta\rangle$ rotating from laboratory to the specific molecular frames, where $[\mathbf{q}^i\rangle = (q_0^i, q_1^i, q_2^i, q_3^i)$, for $i = \alpha,\ \beta$, and $\mathbf{r}$ is the intermolecular vector (with length r). The biaxial GB potential reduces to the standard Gay–Berne[21] when the molecules become uniaxial, and the parameter $\sigma_c = 1\ \sigma_0$, with σ_0 the unit of distance. The explicit expressions for the anisotropic contact term $\sigma(\mathbf{r},\mathbf{Q})$ are related to the geometrical *"contact distance"* (see Ref.[32] for a discussion)

$$\sigma(\mathbf{r},\mathbf{Q}) = r\,\left[2\,\mathbf{r}^T\mathbf{A}^{-1}\mathbf{r}\right]^{-1/2}. \tag{2}$$

The symmetric overlap matrix $\mathbf{A} \equiv \mathbf{A}(\mathbf{Q}) = \mathbf{A}([\mathbf{q}^\alpha\rangle, [\mathbf{q}^\beta\rangle)$ is defined in terms of the diagonal *"shape"* matrix $\mathbf{S}$, with elements $S_{a,b} = \delta_{a,b}\sigma_a$ as

$$\mathbf{A} = \mathbf{M}_\alpha^T\mathbf{S}^2\mathbf{M}_\alpha + \mathbf{M}_\beta^T\mathbf{S}^2\mathbf{M}_\beta, \tag{3}$$

where $\mathbf{M}_i \equiv \mathbf{M}(m_i \leftarrow l) = \mathbf{M}([\mathbf{q}^i\rangle)$ are the cartesian rotation matrices for the two molecules, and which accomplish an active transformation from laboratory to molecular frame (see equation A-4 in the Appendix for their actual computation from the components of the quaternion operators). The anisotropic interaction term is the product of two terms

$$\epsilon(\mathbf{r},\mathbf{Q}) = \epsilon_A^\nu(\mathbf{Q})\epsilon_B^\mu(\mathbf{r},\mathbf{Q}). \tag{4}$$

The dimensionless strength coefficient ϵ_A is

$$\epsilon_A(\mathbf{Q}) = \left[\sigma_x\sigma_y + \sigma_z^2\right]\left[\frac{2\sigma_x\sigma_y}{\det[\mathbf{A}]}\right]^{1/2}, \tag{5}$$

it does explicitly depend on the orientations $\mathbf{Q}$, but not on that of the intermolecular vector, differently from the dimensionless interaction parameter ϵ_B which does

$$\epsilon_B(\mathbf{r},\mathbf{Q}) = 2r^{-2}\,\mathbf{r}^T\mathbf{B}^{-1}\mathbf{r}. \tag{6}$$

The matrix $\mathbf{B} \equiv \mathbf{B}(\mathbf{Q}) = \mathbf{B}([\mathbf{q}^\alpha\rangle, [\mathbf{q}^\beta\rangle)$ is defined in terms of the auxiliary diagonal *"interaction"* matrix $\mathbf{E}$, with elements $E_{a,b} = \delta_{a,b}(\epsilon_0/\epsilon_a)^{1/\mu}$ as

$$\mathbf{B} = \mathbf{M}_\alpha^T\mathbf{E}\mathbf{M}_\alpha + \mathbf{M}_\beta^T\mathbf{E}\mathbf{M}_\beta, \tag{7}$$

where the coefficients ϵ_x, ϵ_y and ϵ_z are related to the well depths for the *side–by–side*, *width–to–width*, and *end–to–end* interactions.[27]

2.3 Torque for the biaxial Gay–Berne potential

The torque acting on molecule measures the gradient of the potential upon an infinitesimal rotation of the molecule itself.[33,34] If the total energy is the sum of pair energies and external field terms, like in here, the total torque acting on a molecule is the vector sum of the torques originated by the single terms. General expressions for the torque (and the gradient) for the family of GB potentials have been reported by Allen and Germano[34] using the methods of Ref.[35] In addition, the expressions for the so–called RE variant[32,36] of the GB potential are given in.[37] Here we give some specialized formulae for the computation of the torque $[\mathbf{G}\rangle$ of the biaxial Gay–Berne potential[22,27] obtained from an alternative derivation based on the angular momentum operator defined in terms of quaternions (given in the Appendix). Since completely symmetrical expressions hold for the torque acting on molecule β by effect of molecule α, to simplify the notation we write the quaternion $[\mathbf{q}\rangle$, the rotation matrix $\mathbf{M}$, and their components without indicating explicitly with an index the specific molecule they refer to. The general definition of the torque measured with respect to the inertial laboratory frame is

$$[\mathbf{G}\rangle = -i\,[\hat{\mathbf{L}}U\rangle, \tag{8}$$

where $[\mathbf{G}\rangle$ is a polar quaternion (see[26] or the Appendix for a definition), and $[\hat{\mathbf{L}}\rangle$ is the angular momentum operator defined with equation A-7 in terms of the components of the four–dimensional orientational gradient $\nabla_q U = (\partial U/\partial q_0, \partial U/\partial q_1, \partial U/\partial q_2, \partial U/\partial q_3)$ with respect to the four components of $[\mathbf{q}\rangle$. Since the computation of the torque requires the evaluation of partial derivatives $\partial U/\partial q_n$, we can write them for the biaxial GB potential as

$$\frac{\partial U(\mathbf{r},\mathbf{Q})}{\partial q_n} = \frac{U(\mathbf{r},\mathbf{Q})}{\epsilon(\mathbf{r},\mathbf{Q})}\frac{\partial \epsilon(\mathbf{r},\mathbf{Q})}{\partial q_n} + 4\epsilon_0 \frac{\epsilon(\mathbf{r},\mathbf{Q})}{\sigma_c}\left[12u^{13}(\mathbf{r},\mathbf{Q}) - 6u^{7}(\mathbf{r},\mathbf{Q})\right]\frac{\partial \sigma(\mathbf{r},\mathbf{Q})}{\partial q_n}. \tag{9}$$

The partial derivatives of the anisotropic contact distance are

$$\frac{\partial \sigma(\mathbf{r},\mathbf{Q})}{\partial q_n} = \frac{\sigma^3(\mathbf{r},\mathbf{Q})}{r^2}\,\mathbf{r}^T\mathbf{A}^{-1}\frac{\partial \mathbf{A}}{\partial q_n}\mathbf{A}^{-1}\mathbf{r}, \tag{10}$$

where we used $(\partial \mathbf{A}\mathbf{A}^{-1}/\partial q_n) = \mathbf{0}$. The derivative of matrix $\mathbf{A}$ with respect to the components of the quaternions $[\mathbf{q}\rangle$ for molecule α is computed in terms of the derivatives of the 3×3 cartesian rotation matrix for the same molecule

$$\frac{\partial \mathbf{A}}{\partial q_n} = \frac{\partial \mathbf{M}^T}{\partial q_n}\mathbf{S}^2\mathbf{M} + \mathbf{M}^T\mathbf{S}^2\frac{\partial \mathbf{M}}{\partial q_n}. \tag{11}$$

The symmetric derivative of $\mathbf{A}$ is recovered as a not–symmetric term summed to its transposed. More explicitly

$$\frac{\partial A_{a,b}}{\partial q_n} = \sum_c \sigma_c^2\left[\frac{\partial M_{c,a}}{\partial q_n}M_{c,b} + M_{c,a}\frac{\partial M_{c,b}}{\partial q_n}\right]. \tag{12}$$

Employing the definition of $\mathbf{M}$ in terms of quaternions (see equation A-4) the computation of the matrices $\partial \mathbf{M}/\partial q_n$ with the partial derivatives with respect to a component q_n is straightforward. The derivative of the anisotropic interaction term is a bit more cumbersome since it involves two different terms

$$\frac{\partial \epsilon(\mathbf{r},\mathbf{Q})}{\partial q_n} = \epsilon(\mathbf{r},\mathbf{Q})\left[\frac{\partial \ln \epsilon_A^{\nu}(\mathbf{Q})}{\partial q_n} + \frac{\partial \ln \epsilon_B^{\mu}(\mathbf{r},\mathbf{Q})}{\partial q_n}\right]. \tag{13}$$

The derivative of first term involves the derivative of a determinant

$$\frac{\partial \ln \epsilon_A^{\nu}(\mathbf{Q})}{\partial q_n} = -\frac{\nu}{2}\frac{1}{\det[\mathbf{A}]}\sum_{a,b,c}\epsilon_{a,b,c}\left[\frac{\partial A_{x,a}}{\partial q_n}A_{y,b}A_{z,c} + A_{x,a}\frac{\partial A_{y,b}}{\partial q_n}A_{z,c} + A_{x,a}A_{y,b}\frac{\partial A_{z,c}}{\partial q_n}\right], \tag{14}$$

where $\epsilon_{a,b,c}$ is the Levi–Civita symbol (permutation symbol) while a, b, c can be x, y or z, and the expression for the derivatives of $\mathbf{A}$ are given by equation 11. The derivative of the second interaction term is instead similar to that of the contact distance

$$\frac{\partial \ln \epsilon_B^{\mu}(\mathbf{r},\mathbf{Q})}{\partial q_n} = -\frac{2\mu}{r^2\epsilon_B(\mathbf{r},\mathbf{Q})}\mathbf{r}^T\mathbf{B}^{-1}\left(\frac{\partial \mathbf{M}^T}{\partial q_n}\mathbf{E}\mathbf{M} + \mathbf{M}^T\mathbf{E}\frac{\partial \mathbf{M}}{\partial q_n}\right)\mathbf{B}^{-1}\mathbf{r}. \tag{15}$$

Assembling these explicit expressions to obtain an equation for the torque allows to integrate the fundamental law of rotational dynamics $[\mathbf{G}\rangle = [\dot{\mathbf{L}}\rangle \equiv \mathrm{d}[\mathbf{L}\rangle/\mathrm{d}t$ relating the torque $[\mathbf{G}\rangle$ to the time derivative of the total angular momentum measured with respect to the inertial laboratory frame. Using a finite differences approach is then possible to obtain the orientational coordinate $[\mathbf{q}\rangle$ and the angular momentum $[\mathbf{L}\rangle$ of each particle at time $t + \Delta t$ given those at time t. The specific technical aspects of this procedure of numerical integration are given in the section (c) of the Appendix.

2.4 Gradient of the biaxial Gay–Berne potential

To solve the equations of translational motion it is necessary to calculate the gradient of the biaxial Gay–Berne potential with respect to the intermolecular vector $\mathbf{r}$, which corresponds to the opposite of the force acting on the center of mass of a particle

$$\nabla_{\mathbf{r}}U(\mathbf{r},\mathbf{Q}) = \frac{U(\mathbf{r},\mathbf{Q})}{\epsilon(\mathbf{r},\mathbf{Q})}\nabla_{\mathbf{r}}\epsilon(\mathbf{r},\mathbf{Q}) - 4\epsilon_0\frac{6\epsilon(\mathbf{r},\mathbf{Q})}{\sigma_c}\left[2u^{13}(\mathbf{r},\mathbf{Q}) - u^{7}(\mathbf{r},\mathbf{Q})\right]\left[\frac{\mathbf{r}}{r} - \nabla_{\mathbf{r}}\sigma(\mathbf{r},\mathbf{Q})\right], \tag{16}$$

where the gradients of the anisotropic contact and interaction terms are

$$\nabla_{\mathbf{r}}\epsilon(\mathbf{r},\mathbf{Q}) = \frac{2\mu\,\epsilon(\mathbf{r},\mathbf{Q})}{r^2}\left[\frac{2}{\epsilon_B(\mathbf{r},\mathbf{Q})}\mathbf{B}^{-1} - 1\right]\mathbf{r}, \tag{17}$$

and

$$\nabla_{\mathbf{r}}\sigma(\mathbf{r},\mathbf{Q}) = \frac{\sigma(\mathbf{r},\mathbf{Q})}{r^2}\left[1 - 2\sigma^2(\mathbf{r},\mathbf{Q})\mathbf{A}^{-1}\right]\mathbf{r}. \tag{18}$$

2.5 External field

A central point of this paper is to consider the effects of an external weak field applied to the BXN system. The simplest (and standard) model used to describe the response of nematic liquid crystals,[38] arises from the mesoscopic dielectric or magnetic anisotropy, which in turn is due to the summing up of microscopic anisotropies. The effective symmetry of the coupling between field and director in a nematic liquid crystal is quadrupolar (i.e. second rank), the energy is invariant under reversal of the director, and the interaction energy scales with the square of the field strength.[38] In nematic materials the first rank contribution to the energy averages to zero. This model is usually sufficient for analyzing electro–optical experimental data, for instance from Kerr effect,[39] or birefringence[40] measurements. Specifically, the interaction of a uniform external field $\mathbf{F}$ (here either the laboratory axes $\mathbf{X}$, $\mathbf{Y}$, or $\mathbf{Z}$) with a single molecule, resulting from its coupling with a certain axis $\mathbf{l}$ (here either the particle axes $\mathbf{l} = \mathbf{x}$, $\mathbf{y}$, or $\mathbf{z}$) is modelled with a second rank Legendre polynomial[38–42,46]

$$U_F = -\xi_F\left[\frac{3}{2}(\mathbf{l}\cdot\mathbf{F})^2 - \frac{1}{2}\right], \tag{19}$$

where $\mathbf{F}$ can be an electric, or a magnetic field, and ξ_F is the coupling parameter measured in ϵ_0 units. As a result of the previous assumptions, this field–coupling model does not consider the additional energy contribution arising from the interaction between induced dipoles, or other local field contributions. To give an estimate

of a conversion factor from simulation to real units we can write the field strength as $E = \sqrt{3\epsilon_0\xi_F/(\varepsilon_0\Delta\varepsilon V_0)}$, where ε_0 is the vacuum permittivity, $\Delta\varepsilon$ the dielectric anisotropy of the liquid crystal, relative to the axis involved, and $V_0 = \pi\sigma_0^3\sigma_x\sigma_y\sigma_z/6$ the molecular volume. Taking as a reference the biaxial mesogens in[1,2] and the parameterization used here and in[10] ($\sigma_x = 1.4\,\sigma_0$, $\sigma_y = 0.714\,\sigma_0$, and $\sigma_z = 3\,\sigma_0$), we can estimate the energy unit from the experimental and simulated nematic–isotropic transition temperatures, i.e. $\epsilon_0 = k_B T_{NI}/T^*_{NI} \approx k_B\,550\;K/3.2$, and the length unit from the molecular dimensions as $\sigma_0 \approx 15$ Å. Since experimental data for biaxial nematics are currently not available, we arbitrarily assume a dielectric anisotropy of 10 for both the axial and transversal switch experiments. To avoid introducing unnecessary complications and specific scaling factors at this stage, we have used the same parameters for all virtual experiments. The switching measurements of Lee *et al.*[20] have been made for a confined sample using specific planar cells and anchoring conditions, but this paper does not address surface effects and considers only the intrinsic properties of a bulk system. With these assumptions and material parameters the electric field results to be $E \approx 120\sqrt{\xi_F}\;\mathrm{V}\,\mu\mathrm{m}^{-1}$, and a coupling parameter $\xi_F = 0.1$ corresponds to $\approx 38\;\mathrm{V}\,\mu\mathrm{m}^{-1}$, a value larger, but of the same order of magnitude of the fields used by Lee *et al.*[20] For every experiment of Figure 1 we have considered the torque generated by the coupling between the space–fixed orientation of the field $\mathbf{F}$ and a molecular axis to give an additional contribution to the total torque (here as a cartesian vector) acting on each molecule as $\mathbf{G}_F = 3\,\xi_F\,(\mathbf{l}\cdot\mathbf{F})\,(\mathbf{l}\times\mathbf{F})$.

3 Computer Experiments

We have performed a series of virtual MD $\pi/2$ director switching experiments on samples formed by $N = 8192$ elongated biaxial GB particles parameterized as in Ref.[10] to have shape and interaction biaxialities of opposite signs, namely $\lambda_\sigma = 0.216$, and $\lambda_\epsilon = -0.060$. The cutoff radius for the GB interaction was $r_c = 4\;\sigma_0$, and using a dimensionless unit mass $m^* = m/m_0 = 1$, the time step was chosen as $\Delta t^* = (\epsilon_0/\sigma_0^2 m_0)^{1/2}\Delta t = 0.001$.

Referring again to molecules similar to those in,[1,2] with relative molecular mass $M_r \approx 800$ amu, this time step is ≈ 0.04 ps. The standard velocity–Verlet integrator[23,24] has been used for the translational equations of motions, while the description of the actual algorithm employed for the equations of rotational motion expressed in quaternions is given in the Appendix. The sample was maintained at constant temperature and pressure by means of the weak coupling thermostat and barostat due to Berendsen,[43] with dimensionless time constants $\tau_T = 1$, and $\tau_P = 100$. The thermodynamic properties, and order parameters of such equilibrium MD samples are entirely consistent with those obtained from earlier MC simulations.[10] Each virtual MD experiment was started from the same well equilibrated configuration in the BXN region of the phase diagram (with $P^* = 8$ and $T^* = 2.8$). The director frame of the starting configuration has been initially aligned with the laboratory axes (given here by the MD sample box sides) using a weak space–fixed field with $\xi_F = 0.05$, which determines an average energy $\langle U_F \rangle$ contributing to less than 0.4% of the total potential energy. The average uniaxial and biaxial order parameters computed from the diagonalization of ordering matrices[8,10] and relevant to the experiment can be defined as ensemble averages of scalar products involving the particle molecular axes and the director frame axes $\mathbf{n}$, $\mathbf{m}$, and $\mathbf{o} = \mathbf{m} \times \mathbf{n}$

$$\langle R^2_{00} \rangle = \left\langle \frac{3}{2} (\mathbf{z} \cdot \mathbf{n})^2 - \frac{1}{2} \right\rangle , \tag{20}$$

$$\langle R^2_{22} \rangle = \left\langle \frac{1}{4} \left[(\mathbf{x} \cdot \mathbf{o})^2 - (\mathbf{x} \cdot \mathbf{m})^2 - (\mathbf{y} \cdot \mathbf{o})^2 + (\mathbf{y} \cdot \mathbf{m})^2 \right] \right\rangle . \tag{21}$$

For our specific system and the thermodynamic state point under study these have average values $\langle R^2_{00} \rangle = 0.787 \pm 0.006$, and $\langle R^2_{22} \rangle = 0.247 \pm 0.008$. We have verified that the weak aligning field determines only a small increase in phase biaxiality $\langle R^2_{22} \rangle$ with respect to the unperturbed equilibrium system, and no measurable effect on the principal order parameter $\langle R^2_{00} \rangle$. Every virtual experiment was started by switching on at a certain time $t = 0$, the external space–fixed uniform field directed along one of the time–zero director frame axes $\mathbf{n}$, $\mathbf{m}$, or $\mathbf{o} = \mathbf{m} \times \mathbf{n}$ (pre–aligned with the laboratory

frame axes $\mathbf{Z}$, $\mathbf{Y}$, and $\mathbf{X}$). Upon turning on the external field each molecule experiences a torque which produces a collective bias in the rotational motion of the particles, and the subsequent overall reorientation of the director reference frame. In Figure 1 we show a scheme with the geometries of the various types of virtual experiments performed in this study.

4 Simulation Results

In analyzing the response of our BXN to the application of the external field (see Figure 1 for actual set up) we concentrate on two aspects: (i) the overall response of the director and its rate of switch, and (ii) the molecular reorganization connected to the switching. Here these two aspects are discussed in turn.

4.1 Director switch

To describe the dynamics of the $\pi/2$ switching experiments we have monitored the time–dependent evolution of the relevant components of the director frame axes, as well as of the order parameters, identified and computed with the algorithm given in,[8] and stored every 20 time steps. For instance, in the experiment of type (C), where the external field is directed along $\mathbf{m}$ and couples to the molecular $\mathbf{x}$ axis, the entire director frame is rotated of $\pi/2$ around $\mathbf{n}$. For this geometry, the relevant observables are the x, and y components of the $\mathbf{m}$ reference axis transforming, with respect to the space fixed laboratory frame, from an initial value close to 0 to a final one close to 1, and from 1 to 0 respectively. Similar choices of relevant components have been made for the other switching geometries of Figure 1. In Figure 2 we show some typical results for three different switching experiments using a field coupling parameter $\xi_F = 0.10\ \epsilon_0$. The pair of solid curves describes the outcome of experiments (C): upon turning on the external field we can see how the initially large m_y component starts decreasing (thick solid line) while m_x increases (thin solid line). At the end of the experiment m_y goes towards

zero, while m_x approaches asymptotically unity. Similar trends can be seen for the other two experiments of type (A) and (B) of Figure 2, where the principal principal director $\mathbf{n}$ is rotated (dashed, and dotted curves). In these cases, there are two possible switching geometries in the bulk phase, where either the molecular $\mathbf{x}$, or $\mathbf{y}$ axes are coupled to the field (see schemes (A) and (B) of Figure 1). The two experiments involve different transversal directions and are quantitatively different because of the molecular and phase biaxiality. The switching times involving the coupling of the field with the molecular axis perpendicular to the largest face are constantly the highest, as is the case in type (B) experiments where a larger volume of fluid needs to be displaced by pushing away nearby molecules to complete each particle rotation. It is clear from the paradigmatic results of Figure 2 that the secondary director realignment is quite faster than the other.

These curves were very well fitted with a logistic, sigmoidal type, function

$$f(t) = \exp[b\,(t-a)]/(1+\exp[b\,(t-a)]), \tag{22}$$

with the optimal parameters a, and b obtained by chi–square minimization using the classical simplex algorithm of Nelder and Mead.[44] We have then arbitrarily defined the switching times t_s as those required to the fitted director component to become larger than 0.95 (if increasing) or smaller than 0.05 (if decreasing). In Figure 3 we show the results for these switching times as obtained for the various experiments. Although the absolute switching times are not available from our generic type simulation based on the generalized Gay-Berne model, their relative values should be reliably assessed. Notably, the reorientation of the secondary $\mathbf{m}$ director is faster than that of the principal one $\mathbf{n}$ by approximatively one order of magnitude. For the family of switching experiments addressed by this study we have not found, as expected on the grounds of symmetry of the experiments, a systematic anisotropy for the coupling of a transversal field with the molecular $\mathbf{x}$, or $\mathbf{y}$ axes, and the reorientation time of $\mathbf{m}$ is practically the same in both (C) and (D) cases.

4.2 Molecular reorganization under field switching

From a naïve point of view, possibly comforted by the smooth change in director component evolution (see Figure 2) the effect of a switching field could be expected to be just that of rotating the sample as a whole. However, this is not always the case, as shown by experiments[40,42,45] and simulations.[46,47,49] Thus, although the expectation for a nematic is that of uniform rotation as a monodomain, for smectics this process occurs for director–field angles below 45°, while a complex reorganization occurs when the angle is 90°. To examine changes of orientational organization in our BXN samples, we have monitored the time evolution of the uniaxial and biaxial order parameters (see equations 20 and 21). Since $R^2_{00}(t)$, and $R^2_{22}(t)$ refer to the instantaneous director frame, they should be constant if the sample reorients as a whole. In Figure 4 we report as an example these time evolutions for the transversal (biaxial) switching experiment of Figure 1–(C). We see that in the transversal switching experiments the final value of the $R^2_{00}(t)$ order parameter, is slightly increased ($\approx 8\%$ for $\xi_F = 1$), while for the weaker couplings ($\xi_F \leq 0.2$) it is practically unaffected. The field application induces a temporary disappearing of the biaxial ordering (i.e. a dip in the $R^2_{22}(t)$ plots of Figure 4–b) which is reversibly recovered after the relaxation of the molecular organization, albeit to a higher value (see Figure 4–a). This indicates that for these experiments, transversal switching appears to proceed with just a single regime for all field strengths, but also that this process does not take place with an overall rotation, but rather via localized biaxial domain reorientations, causing first the overall phase biaxiality to be momentarily destroyed, with its recovery only at the end of the switching process, when the long–range correlation between domains are restored. At the same time, the orientation of the $\mathbf{n}$ director axis is stable during the experiment and only mildly affected by the switching field (see Figure 4–b). A direct visualization of this process is shown in Figure 5 where we present four MD sample snapshots taken at different times for this type (C) experiment with field strength $\xi_F = 0.10$. The particle orientations are color coded to make it easier to appreciate the change in direction of the molecular $\mathbf{y}$ axis

with respect to the laboratory **X** axis, which is the direction of the applied field. We see that the intermediate Figure 5–b configuration (corresponding to the dip in $R^2_{22}(t)$ in Figure 4–b) shows a non uniform distribution of transversal orientations and several biaxial domains. The uniform phase biaxiality is almost recovered in snapshot Figure 5–d which has been taken at the end of the order parameter dip of Figure 4–b.

Considering now a main director switching, in the plots of Figure 6 we see the order parameters dynamics for the type (B) experiment of Figure 1. For this geometry the instantaneous principal order parameter $R^2_{00}(t)$ and the phase biaxiality $R^2_{22}(t)$ are essentially constant for the smaller field strengths (up to $\xi_F = 0.2$), while they exhibit an initial decrease followed by a rapid recovery to the initial values for the higher coupling values $\xi_F = 0.5$, and 1.0. For these experiments we see that the dynamic regimes are different from the previous (transversal) one and we observe two different types of behavior. For the weaker fields the orientational structure of the biaxial phase is conserved throughout the experiments, and the switching appears to take place through a collective concerted reorientation of the whole sample (i.e. **n**), while **m** remains unaffected. For the stronger fields instead the larger temporarily coupling destroys the long range correlations, and the degree of orientational ordering during the experiment decreases both with respect to **n** and **m** and we observe in Figure 6 the falling values of $R^2_{00}(t)$ and $R^2_{22}(t)$. The uniform structure of the BXN liquid sample breaks down into uncorrelated but still locally aligned domains. Even in this case the long range orientational correlations are recovered towards the end of the experiments. The snapshots of Figures 7 and 8 provide a concrete example of these two regimes. In Figure 7 we see that at all times all particles are homogeneously aligned with respect to a common principal director **n** which continuously rotates so as to eventually align with the external field at the end of the experiment. On the contrary, in Figure 8 the intermediate snapshots show the formation of uniformly oriented domains which align with respect to the field with different rates, and a uniform distribution of orientations is recovered only for snapshot Figure 8–d.

5 Conclusions

We have shown that a biaxial nematic can respond effectively to an applied external field allowing a change of the direction of the principal and secondary directors and that the latter $\pi/2$ switching is up to an order of magnitude faster than the former one. This is an essential feature of future BXN based electro–optical devices and displays and, even though our molecular dynamics experiments were performed on model systems and in bulk, thus neglecting surface and anchoring effects, we believe the result to be encouraging from the point of view of future applications.

We have also shown that the process of realignment of the BXN following the switch can involve a reorganization of the molecular orientational structure in the liquid phase, rather than a simple uniform reorientation. This process should be amenable to experimental tests, e.g. using NMR[42] or optical techniques. It seems clear that MD simulation of biaxial devices can be a useful complement to theory and experiment, both in explaining and predicting the behavior of these complex anisotropic systems.

6 Acknowledgements

We thank MUR (PRIN *"Modelling and characterization of liquid crystals for nano–organized structures"* #2005035119 2006–2007), and INSTM (PRISMA *"Software architecture for nanomaterials designs: an integrated environment"*) for financial support.

Appendix

In this Appendix we give some relevant expressions for the: (a) angular momentum operator $\hat{\mathbf{L}}$, and torque $\mathbf{G}$ in terms of a quaternionic representation of molecular orientations; (b) kinematic and dynamic equations of rotational motion in terms of a quaternionic representation; (c) velocity–Verlet–like integrator of the rotational equations of motions for a rigid body used in this study. To begin with we summarize the properties of quaternions.

Quaternions

A molecular dynamics simulation of rigid bodies using quaternions is appealing since the equations of rotational motion are free of singularities.[50,51]

Even if extensive and detailed discussions of quaternion algebra, and the relation with the three dimensional rotation groups can be found e.g. in,[26] we think it is convenient to introduce the notation used, and give a short recapitulation of quaternion properties and algebra. All rotations are considered active, and the convention used for angles, rotations, and quaternions is that of Altmann,[26] which coincides with that of Rose,[52] and Brink and Satchler[53] for Euler angles, and consequently that of Zannoni and Guerra[30] for quaternions.

A quaternion $[\mathbf{q}\rangle = (q_0, q_1, q_2, q_3)$[26] is a unitary operator $\hat{R}(\phi\mathbf{n})$ which rotates a tensorial quantity of rank 1/2 of an angle ϕ with respect to a three–dimensional unit vector $\mathbf{n} = (n_x, n_y, n_z)$, and it can be written in a matrix representation as a 4×1 column with components $q_0 = \cos(\phi/2)$, $q_1 = n_x \sin(\phi/2)$, $q_2 = n_y \sin(\phi/2)$, and $q_3 = n_z \sin(\phi/2)$.

The product of two quaternions $[\mathbf{c}\rangle = [\mathbf{a}\rangle[\mathbf{b}\rangle \equiv [\mathbf{a}][\mathbf{b}\rangle$, i.e. the composition of two successive rotations, is a quaternion itself, and using a matrix product can be written as

$$[\mathbf{c}\rangle = \begin{bmatrix} +a_0 & -a_1 & -a_2 & -a_3 \\ +a_1 & +a_0 & -a_3 & +a_2 \\ +a_2 & +a_3 & +a_0 & -a_1 \\ +a_3 & -a_2 & +a_1 & +a_0 \end{bmatrix} \begin{bmatrix} b_0 \\ b_1 \\ b_2 \\ b_3 \end{bmatrix} = [\mathbf{a}][\mathbf{b}\rangle. \tag{A-1}$$

Quaternions representing (unitary) rotation operators are normalized to one as $\langle\mathbf{a}][\mathbf{a}\rangle = [\mathbf{a}\rangle^T[\mathbf{a}\rangle = \sum_i a_i^2 = 1$. The inverse of a quaternion $[\mathbf{q}\rangle^{-1} = [-\mathbf{q}\rangle$ has the property $[\mathbf{q}]^{-1}[\mathbf{q}\rangle = [\mathbf{q}]^T[\mathbf{q}\rangle = [-\mathbf{q}][\mathbf{q}\rangle = [1\rangle$, where $[-\mathbf{q}\rangle = (q_0, -q_1, -q_2, -q_3)$ performs a rotation of an angle $-\phi$ around the axis $\mathbf{n}$, and $[1\rangle$ is the identity operator, i.e. a column matrix with $(1, 0, 0, 0)$ elements. Any three–dimensional vector $\mathbf{r} = (r_x, r_y, r_z)$ can be considered as an axial quaternion $|\mathbf{r}\rangle$, whose first component $q_0 = 0$, and $q_1 = r_x$, $q_2 = r_y$, and $q_3 = r_z$, such that $\mathbf{r} = \text{pole–of}\{[\mathbf{r}\rangle\}$. The unitary operator pole–of extracts the vector part from an axial quaternion.[26] Since in general $\langle\mathbf{r}][\mathbf{r}\rangle \neq 1$, the quaternion $[\mathbf{r}\rangle$ is not a rotation operator.

The operator which rotates a vector (i.e. a rank 1 tensor) from laboratory (i.e. space–fixed, aka inertial) frame to molecular (i.e. body–fixed, aka local, e.g. the one defined by the eigenvectors of the inertia tensor) frame $\mathbf{r}_m = \hat{R}(m \leftarrow l)\,\mathbf{r}$ is obtained from the conical transformation linking the two systems as[26]

$$[\mathbf{r}_m\rangle = [\mathbf{q}]^T[\mathbf{r}][\mathbf{q}\rangle = [\mathbf{M}][\mathbf{r}\rangle. \tag{A-2}$$

The 4×4 rotation matrix $[\mathbf{M}]$ has a block structure

$$[\mathbf{M}] = \left[\begin{array}{c|c} 1 & \mathbf{0} \\ \hline \mathbf{0} & \mathbf{M} \end{array}\right]. \tag{A-3}$$

where the 3×3 minor relative to the element $[\mathbf{M}]_{1,1}$ is the correspondent cartesian rotation matrix $\mathbf{M}(m \leftarrow l)$[52,53] which performs the active rotation of a rank one tensor from laboratory to molecular frame (e.g. $\mathbf{r}_m = \mathbf{M}\,\mathbf{r}$)

$$\mathbf{M} = \begin{bmatrix} 1-2q_2^2-2q_3^2 & 2q_1q_2+2q_0q_3 & 2q_1q_3-2q_0q_2 \\ 2q_1q_2-2q_0q_3 & 1-2q_3^2-2q_1^2 & 2q_2q_3+2q_0q_1 \\ 2q_1q_3+2q_0q_2 & 2q_2q_3-2q_0q_1 & 1-2q_2^2-2q_1^2 \end{bmatrix}. \tag{A-4}$$

(a) Angular momentum operator

The angular momentum operator $\hat{\mathbf{L}}$ can be derived from the expression of an infinitesimal rotation $\delta\phi$ around an axis $\mathbf{n}$.[26,30,52]

$$\hat{R}(\delta\phi\,\mathbf{n}) = \exp\left(-i\delta\phi\,(\mathbf{n}\cdot\hat{\mathbf{L}})\right). \tag{A-5}$$

The angular momentum operator in a quaternion representation is

$$[\hat{\mathbf{L}}^{(q)}\rangle = -\frac{1}{2}i[\nabla_q - \mathbf{q}\,g_q\rangle, \qquad \text{with } g_q = \langle\mathbf{q}][\nabla_q\rangle = \sum_q q_n(\partial/\partial q_n), \tag{A-6}$$

where $\nabla_q = (\partial/\partial q_0, \partial/\partial q_1, \partial/\partial q_2, \partial/\partial q_3)$ is the four–dimensional orientational gradient. The Lagrange multiplier g_q enforces the quaternion normalization constraint and produces a conditional derivative tangent to the unit four–dimensional sphere. Expressions for the angular momentum operator $\hat{\mathbf{L}}$ in terms of quaternions have also been reported, e.g. by Allen[54] (using the convention of Goldstein[31]). The same operator written with respect to the laboratory frame is

$$[\hat{\mathbf{L}}\rangle = [\hat{\mathbf{L}}^{(q)}][-\mathbf{q}\rangle. \tag{A-7}$$

The cartesian angular momentum operator is

$$\hat{\mathbf{L}} = \left(\hat{L}_x, \hat{L}_y, \hat{L}_z\right) = \text{pole–of}\left\{[\hat{\mathbf{L}}\rangle\right\}. \tag{A-8}$$

(b) Kinematic and dynamic equations of rotational motion

The kinematic equation of motion linking the angular velocity (measured with respect to the laboratory frame) with the time derivatives of the components of the rotation

operator is[50,51,55]

$$[\dot{\mathbf{q}}\rangle = (1/2)[\boldsymbol{\omega}][\mathbf{q}\rangle. \tag{A-9}$$

Both angular velocity

$$[\boldsymbol{\omega}\rangle = [\mathbf{M}]^T[\mathbf{I}_m]^{-1}[\mathbf{M}][\mathbf{L}\rangle, \tag{A-10}$$

and angular momentum

$$[\mathbf{L}\rangle = 2[\mathbf{M}]^T[\mathbf{I}_m][\mathbf{q}]^T[\dot{\mathbf{q}}\rangle, \tag{A-11}$$

are polar quaternions defined in terms of the cartesian angular velocity $\boldsymbol{\omega}$ and angular momentum $\mathbf{L}$, which in turn can be computed during the MD trajectory at every discrete time from the orientation $[\mathbf{q}\rangle$ and the velocity $[\dot{\mathbf{q}}\rangle$. The inertia tensor $[\mathbf{I}_m]$ measured with respect to the molecular frame, has the top left diagonal element $[\mathbf{I}_m]_{1,1} = 1$, while its 3×3 minor is a diagonal matrix $\mathbf{I}_m$ whose elements are the eigenvalues I_{xx}, I_{yy}, and I_{zz} of the inertia tensor

$$[\mathbf{I}_m] = \left[\begin{array}{c|c} 1 & \mathbf{0} \\ \hline \mathbf{0} & \mathbf{I}_m \end{array}\right], \tag{A-12}$$

The dynamical equations giving the time evolution of the orientation $[\mathbf{q}\rangle$, and the angular momentum $[\mathbf{L}\rangle$ can be determined considering the single molecule Liouville operators $\hat{\mathbf{U}}_\mathbf{q}$, and $\hat{\mathbf{U}}_\mathbf{L}$ defined as[24,56]

$$i\hat{\mathbf{U}}_\mathbf{q} = \langle\dot{\mathbf{q}}][\nabla_q - g_q\mathbf{q}\rangle, \tag{A-13}$$

and

$$i\hat{\mathbf{U}}_\mathbf{L} = \langle\mathbf{G}][\nabla_L\rangle, \tag{A-14}$$

where the four–dimensional gradient $[\nabla_L\rangle = (\partial/\partial L_0, \partial/\partial L_1, \partial/\partial L_2, \partial/\partial L_3)$. The effect of the unitary operator $\exp\left(i\Delta t\,\hat{\mathbf{U}}_{\mathbf{q}}\right) = \exp\left(\Delta t\,\langle\dot{\mathbf{q}}][\nabla_q - g_q\mathbf{q}\rangle\right)$ is that of evolving of a time step the orientation from the value at t to that at $t+\Delta t$ by means a finite rotation of the quaternion. Within a first–order approximation we have

$$\exp\left(i\Delta t\,\hat{\mathbf{U}}_{\mathbf{q}}\right)[\mathbf{q}\rangle \approx \cos(\dot{q}\Delta t)[\mathbf{q}\rangle + \Delta t\, j_0(\dot{q}\Delta t)[\dot{\mathbf{q}}\rangle, \tag{A-15}$$

where $j_0(x) = \sin(x)/x$ is the rank zero spherical Bessel function of the first kind, with the purpose of avoiding numerical problems for $\dot{q} \to 0$. This results is essentially the core of the algorithm proposed by Matubayasi and Nakahara in[25] (see also[57,58] for detailed discussions on the properties and stability of the integrators based on this evolution operator). The effect of the unitary operator $\exp\left(i\Delta t\,\hat{\mathbf{U}}_{\mathbf{L}}\right) = \exp\left(\Delta t\,\langle\dot{\mathbf{L}}][\nabla_L\rangle\right)$ is instead that of evolving the angular momentum from t to $t+\Delta t$

$$\exp\left(i\Delta t\,\hat{\mathbf{U}}_{\mathbf{L}}\right)[\mathbf{L}\rangle \approx [\mathbf{L}\rangle + \Delta t\,[\mathbf{G}\rangle. \tag{A-16}$$

This is also the approximated solution of $[\dot{\mathbf{L}}\rangle = [\mathbf{G}\rangle$ given by the Euler method of solution of differential equations. The total single molecule Liouville operator is $\hat{\mathbf{U}} = \hat{\mathbf{U}}_{\mathbf{q}} + \hat{\mathbf{U}}_{\mathbf{L}}$, and it defines the finite difference propagator $\exp\left(i\Delta t\,(\hat{\mathbf{U}}_{\mathbf{q}} + \hat{\mathbf{U}}_{\mathbf{L}})\right)$ which can be approximated using a Trotter factorization to produce a time reversible symplectic integrators.[24,56]

(c) Propagator/integrator of rotational equations of motion

The starting point of the evolution algorithm are the dynamical variables specifying for every molecule the orientation $[\mathbf{q}(0)\rangle$, and the angular momentum $[\mathbf{L}(0)\rangle$ at a certain time $t = 0$. From these dynamical variables it is possible to compute the angular velocity $[\dot{\mathbf{q}}(0)\rangle$ through the kinematic equations A-9 and A-10 given earlier.

The time evolution by a discrete time–step Δt is accomplished with the following scheme (which produces a velocity–Verlet–like algorithm[25,58]):

(1) Half time–step evolution of the angular momentum

$$[\mathbf{L}(\Delta t/2)\rangle = [\mathbf{L}(0)\rangle + (\Delta t/2)[\mathbf{G}(0)\rangle, \tag{A-17}$$

where the torque $[\mathbf{G}(0)\rangle$ is a function of the orientation $[\mathbf{q}(0)\rangle$. Once $[\mathbf{L}(\Delta t/2)\rangle$ is known, the half–integer time–step orientation is estimated from $[\dot{\mathbf{q}}(0)\rangle$ as

$$[\mathbf{q}(\Delta t/2)\rangle = \cos(\dot{q}(0)\Delta t/2)[\mathbf{q}(0)\rangle + (\Delta t/2)\, j_0(\dot{q}(0)\Delta t/2)[\dot{\mathbf{q}}(0)\rangle, \tag{A-18}$$

and the half–integer time–step angular velocity (necessary to perform the following step) is computed as

$$[\dot{\mathbf{q}}(\Delta t/2)\rangle = (1/2)[\mathbf{q}(\Delta t/2)][\mathbf{I}_m]^{-1}[\mathbf{q}(\Delta t/2)]^T[\mathbf{L}(\Delta t/2)][\mathbf{q}(\Delta t/2)\rangle. \tag{A-19}$$

(2) Whole time–step evolution of the orientation

$$[\mathbf{q}(\Delta t)\rangle = \cos(\dot{q}(\Delta t/2)\Delta t)[\mathbf{q}(0)\rangle + \Delta t\, j_0(\dot{q}(\Delta t/2)\Delta t)[\dot{\mathbf{q}}(\Delta t/2)], \tag{A-20}$$

and from this orientation the torque $[\mathbf{G}(\Delta t)\rangle$ is calculated.

(3) Half time–step evolution of the angular momentum

$$[\mathbf{L}(\Delta t)\rangle = [\mathbf{L}(\Delta t/2)\rangle + (\Delta t/2)[\mathbf{G}(\Delta t)\rangle, \tag{A-21}$$

and from $[\mathbf{q}(\Delta t)\rangle$ and $[\mathbf{L}(\Delta t)\rangle$ it is possible to compute $[\dot{\mathbf{q}}(\Delta t)]$ inverting equation A-11 as $[\dot{\mathbf{q}}\rangle = [\mathbf{q}][\mathbf{I}_m]^{-1}[\mathbf{M}][\mathbf{L}\rangle/2$ and complete the time evolution cycle.

In the limit of $\Delta t \to 0$ equation A-20 is consistent with the $[\mathbf{q}][\dot{\mathbf{q}}\rangle = 0$ constraint. To improve numerical accuracy when using longer times steps it may be convenient to actually enforce this constraint in the MD code, even though this destroys the time reversibility property of the integrator.[25,58] This orientation propagator has been embedded in a simple multiple time step scheme[56] with a standard velocity–Verlet propagator for the translational motion to achieve an algorithm for the complete finite differences integration of the full equations of motion for a rigid body.[58]

References

[1] L. Madsen, T. Dingemans, M. Nakata and E. Samulski, Phys. Rev. Lett. **92**, 145505 (2004).

[2] B. Acharya, A. Primak and S. Kumar, Phys. Rev. Lett. **92**, 145506 (2004).

[3] K. Merkel, A. Kocot, J. K. Vij, R. Korlacki, G. H. Mehl and T. Meyer, Phys. Rev. Lett. **93**, 237801 (2004).

[4] K. Severing and K. Saalwachter, Phys. Rev. Lett. **92**, 125501 (2004).

[5] J. L. Figueirinhas, C. Cruz, D. Filip, G. Feio, A. C. Ribeiro, Y. Frere, T. Meyer and G. H. Mehl, Phys. Rev. Lett. **94**, 107802 (2005).

[6] M. Freiser, Phys. Rev. Lett. **24**, 1041 (1970).

[7] M. Allen, Liq. Cryst. **8**, 499 (1990).

[8] F. Biscarini, C. Chiccoli, P. Pasini, F. Semeria and C. Zannoni, Phys. Rev. Lett. **75**, 1803 (1995).

[9] K. Neupane, S. W. Kang, S. Sharma, D. Carney, T. Meyer, G. H. Mehl, D. W. Allender, S. Kumar and S. Sprunt, Phys. Rev. Lett. **97**, 207802 (2006).

[10] R. Berardi and C. Zannoni, J. Chem. Phys. **113**, 5971 (2000).

[11] J. Peláez and M. Wilson, Phys. Rev. Lett. **97** (2006).

[12] G. De Matteis, S. Romano and E. Virga, Phys. Rev. E **72**, 04170 (2005).

[13] L. Longa and H. R. Trebin, Liq. Cryst. **5**, 617 (1989).

[14] L. Longa, J. Stelzer and D. Dunmur, Mol. Cryst. Liq. Cryst. **323**, 191 (1998).

[15] L. Longa, J. Stelzer and D. Dunmur, J. Chem. Phys. **109**, 1555 (1998).

[16] D. Baalss, Z. Naturfors. Sect. A-J. Phys. Sci. **45**, 7 (1990).

[17] M. Fialkowski, Phys. Rev. E **58**, 1955 (1998).

[18] T. Carlsson and F. Leslie, Liq. Cryst. **10**, 325 (1991).

[19] C. Zannoni, J. Mat. Chem. **11**, 2637 (2001).

[20] J. Lee, T. Lim, W. Kim and J. Jin, J. Appl. Phys. **101**, 034105 (2007).

[21] J. G. Gay and B. J. Berne, J. Chem. Phys. **74**, 3316 (1981).

[22] R. Berardi, C. Fava and C. Zannoni, Chem. Phys. Lett. **236**, 462 (1995).

[23] M. P. Allen and D. J. Tildesley, *Computer Simulation of Liquids* (Oxford University Press, Walton Street, Oxford OX2 6DP, 1989).

[24] D. Frenkel and B. Smit, *Understanding Molecular Simulations, 2nd edition* (Academic Press, San Diego, 2001).

[25] N. Matubayasi and M. Nakahara, J. Chem. Phys. **110**, 3291 (1999).

[26] S. Altmann, *Rotations, Quaternions, and Double Groups* (Clarendon Press, Oxford, 1986).

[27] R. Berardi, C. Fava and C. Zannoni, Chem. Phys. Lett. **297**, 8 (1998).

[28] M. R. Wilson, Int. Rev. Phys. Chem. **24**, 421 (2005).

[29] C. M. Care and D. J. Cleaver, Rep. Prog. Phys. **68**, 2665 (2005).

[30] C. Zannoni and M. Guerra, Mol. Phys. **44**, 143 (1981).

[31] H. Goldstein, *Classical Mechanics* (Addison–Wesley, Reading MA, 1980).

[32] R. Everaers and M. R. Ejtehadi, Phys. Rev. E **67**, 041710 (2003).

[33] A. J. Stone, Mol. Phys. **36**, 241 (1978).

[34] M. P. Allen and G. Germano, Mol. Phys. **104**, 3225 (2006).

[35] S. L. Price, A. J. Stone and M. Alderton, Mol. Phys. **52**, 987 (1984).

[36] M. Babadi, R. Everaers and M. R. Ejtehadi, J. Chem. Phys. **124**, 174708 (2006).

[37] M. Babadi, M. R. Ejtehadi and R. Everaers, J. Comput. Phys. **219**, 770 (2006).

[38] W. de Jeu, *Physical Properties of Liquid Crystalline Materials* (Gordon and Breach, New York, 1980).

[39] J. Hanus, Phys. Rev. **178**, 420 (1969).

[40] I. Lelidis, M. Nobili and G. Durand, Phys. Rev. E **48**, 3818 (1993).

[41] E. Berggren, C. Zannoni, C. Chiccoli, P. Pasini and F. Semeria, Phys. Rev. E **49**, 614 (1994).

[42] G. R. Luckhurst, Mol. Cryst. Liq. Cryst. **347**, 365 (2000).

[43] H. J. C. Berendsen, J. P. M. Postma, W. F. van Gunsteren, A. Di Nola and J. R. Haak, J. Chem. Phys. **81**, 3684 (1984).

[44] J. A. Nelder and R. Mead, Comput. J. **7**, 308 (1965).

[45] G. R. Luckhurst, T. Miyamoto, A. Sugimura and B. A. Timimi, Mol. Cryst. Liq. Cryst. **347**, 391 (2000).

[46] G. R. Luckhurst, T. Miyamoto, A. Sugimura and B. A. Timimi, J. Chem. Phys. **112**, 4342 (2000).

[47] G. R. Luckhurst and K. Satoh, Mol. Cryst. Liq. Cryst. **394**, 153 (2003).

[48] G. R. Luckhurst and K. Satoh, Mol. Cryst. Liq. Cryst. **402**, 321 (2003).

[49] R. Berardi, S. Orlandi and C. Zannoni, Mol. Cryst. Liq. Cryst. **394**, 141 (2003).

[50] D. J. Evans, Mol. Phys. **34**, 317 (1977).

[51] D. J. Evans and S. Murad, Mol. Phys. **34**, 327 (1977).

[52] M. E. Rose, *Elementary Theory of Angular Momentum* (Wiley, New York, 1957).

[53] D. Brink and G. Satchler, *Angular Momentum* (Clarendon Press, Oxford, U.K., 1968), 2nd ed.

[54] M. P. Allen, Mol. Phys. **52**, 717 (1984).

[55] G. S. Pawley, Mol. Phys. **43**, 1321 (1981).

[56] M. E. Tuckerman, B. J. Berne and G. J. Martyna, J. Chem. Phys. **97**, 1990 (1992).

[57] T. F. Miller III, M. Eleftheriou, P. Pattnaik, A. Ndirango, D. Newns and G. J. Martyna, J. Chem. Phys. **116**, 8649 (2002).

[58] H. Kamberaj, R. J. Low and M. P. Neal, J. Chem. Phys. **122**, 224114 (2005).

Figure 1: (Color online) The geometry of the principal (A), (B), and secondary (C), (D) switching experiments described in the text: the director axes are labelled $\mathbf{n}$, $\mathbf{m}$, and $\mathbf{o} = \mathbf{m} \times \mathbf{n}$ (not shown here), while the external field $\mathbf{F}$ couples in turn with the molecular $\mathbf{x}$, $\mathbf{y}$, or $\mathbf{z}$ axes and generates the torque $\mathbf{G}$.

Figure 2: (Color online) Dynamics of the field induced reorientation of the principal ($\mathbf{n}$) and secondary ($\mathbf{m}$) director axes of the BXN phase for the experiments of type (A) (dashed), (B) (dotted), and (C) (solid) of Figure 1, for an external field of magnitude $\xi_F = 0.10\ \epsilon_0$. Each experiment is described by a pair of intersecting curves (one thin, the other thick) with the same drawing style. These lines represent the evolution of selected components of a director axis (with respect to the space fixed frame) whose values are exchanged by the experiment. Thin (thick) lines are the components parallel (perpendicular) to the field at the beginning of the experiment.

Figure 3: (Color online) The $\log_{10}$ plot of the principal (A), (B). and secondary (C), (D) switching times t_S for various commutation experiments of Figure 1, with field module $\xi_F = 0.10$, 0.20, 0.50, and 1.00 ϵ_0.

Figure 4: (Color online) Dynamics of the instantaneous: (a) uniaxial $R^2_{00}(t)$; and (b) biaxial $R^2_{22}(t)$ order parameters for the transversal switch, type (C) experiments with field $\mathbf{m}$, coupled to molecular axis $\mathbf{x}$.

Figure 5: Snapshots of BXN samples relative to a short axis switch virtual experiment of type (C) with field $\xi_F = 0.10$, showing biaxiality disappearance. The snapshots are as viewed from the $\mathbf{Y}$ laboratory axis and have been taken at time steps: (a) $t/\Delta t = 0$; (b) 40000; (c) 60000; and (d) 100000. The particle orientations are color coded according to the palette shown (e), with $\cos\beta = \mathbf{y} \cdot \mathbf{X}$.

Figure 6: (Color online) Dynamics of the instantaneous: (a) uniaxial $R^2_{00}(t)$; and (b) biaxial $R^2_{22}(t)$ order parameters for longitudinal switch, the type (B) experiments with field $\mathbf{m}$, coupled to molecular axis $\mathbf{z}$.

Figure 7: Snapshots of BXN samples relative to a long axis switch virtual experiment of type (B) with relatively weak field ($\xi_F = 0.10$), showing whole sample rotation. The snapshots are as viewed from the $\mathbf{X}$ laboratory axis and have been taken at time steps: (a) $t/\Delta t = 0$; (b) 160000; (c) 240000; and (d) 320000. The particles orientations are color coded according to the palette shown (e), with $\cos\beta = \mathbf{z} \cdot \mathbf{Y}$.

Figure 8: Snapshots of BXN samples relative to a long axis switch virtual experiment of type (B) with strong field ($\xi_F = 0.50$), showing order disruption. The snapshots are as viewed from the $\mathbf{X}$ laboratory axis and have been taken at time steps: (a) $t/\Delta t = 0$; (b) 40000; (c) 60000; and 80000(d). The particle orientations are color coded according to the palette shown (e), with $\cos\beta = \mathbf{z} \cdot \mathbf{Y}$.

Figure 1

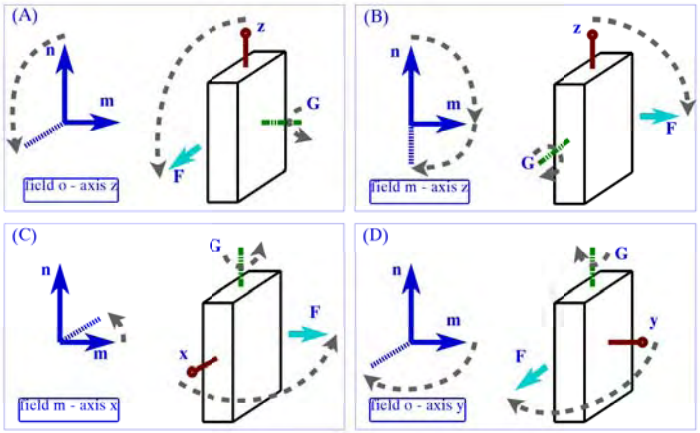

Figure 2

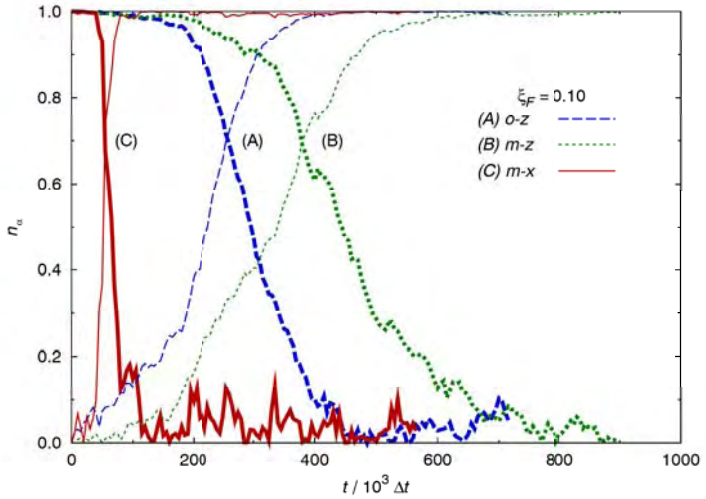

Figure 3

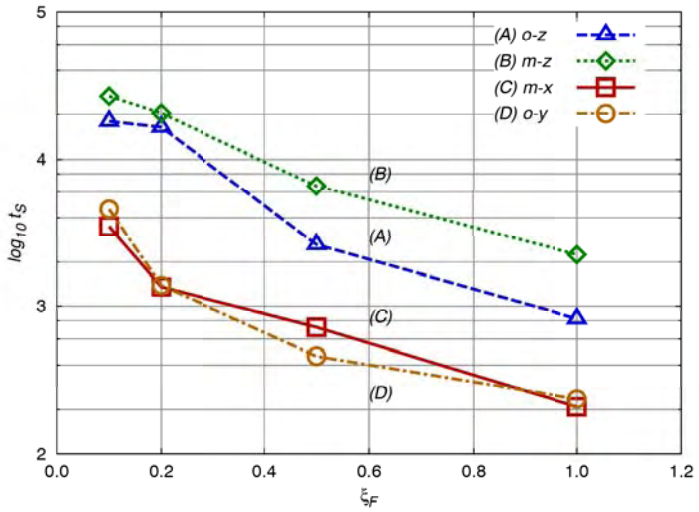

Figure 4

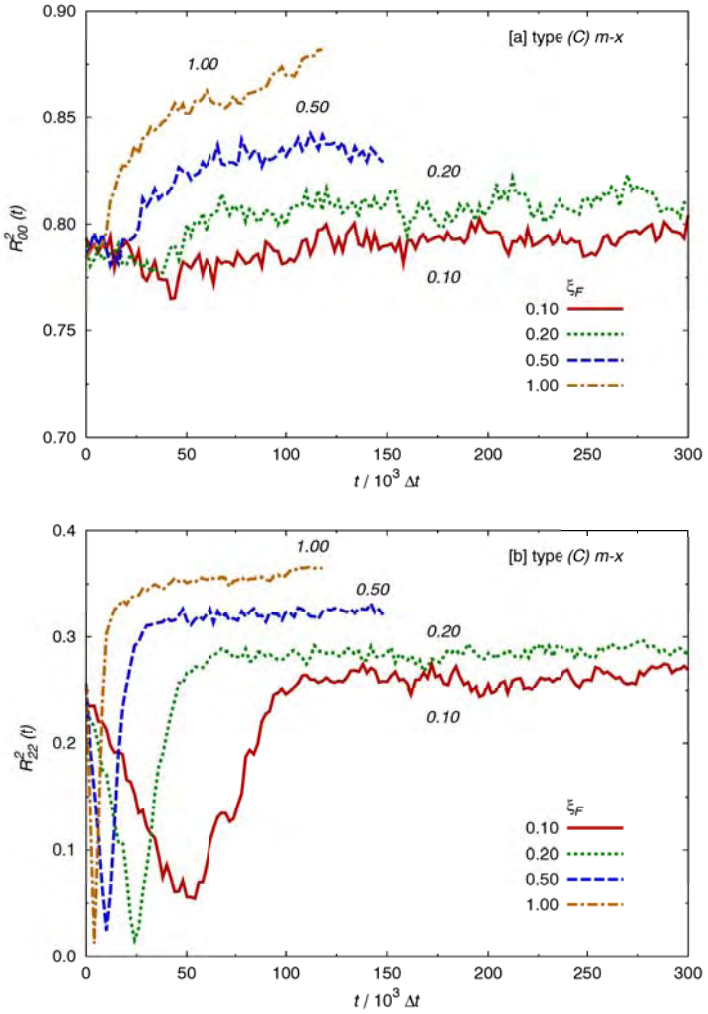

Figure 5

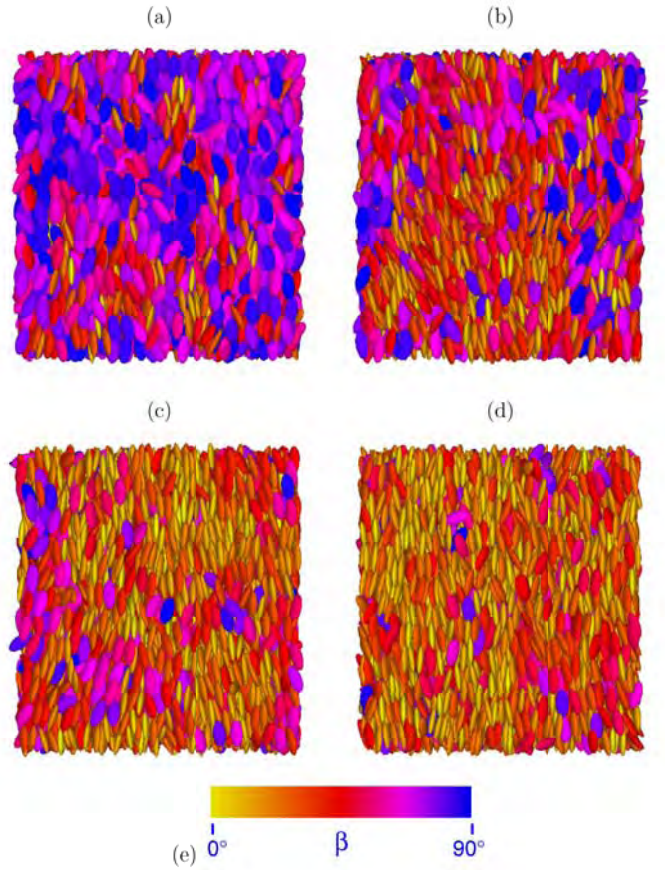

Figure 6

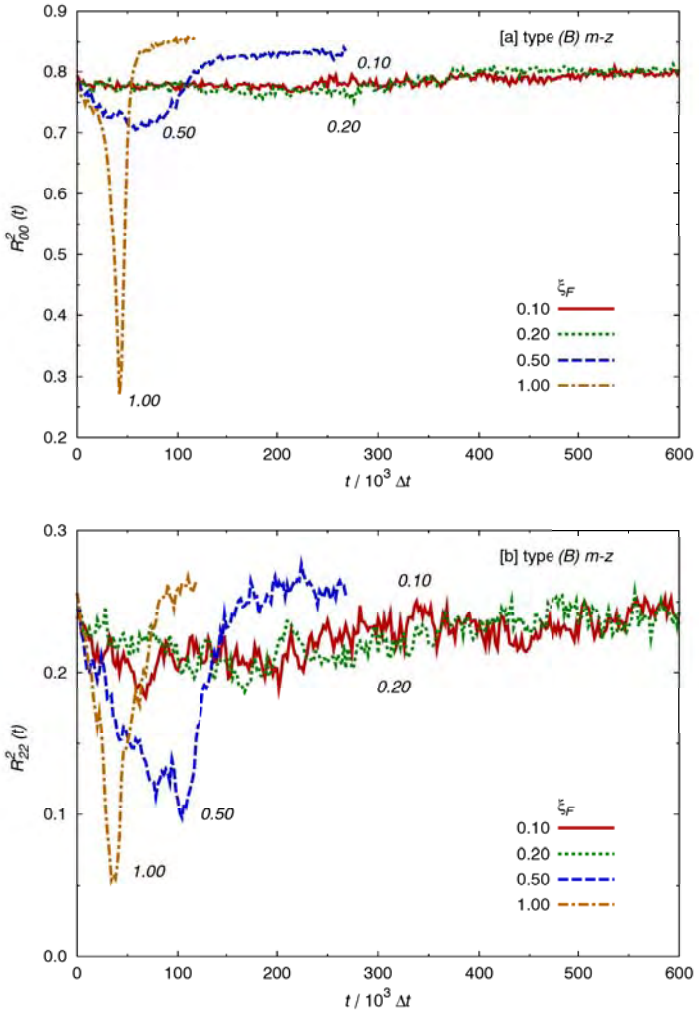

Figure 7

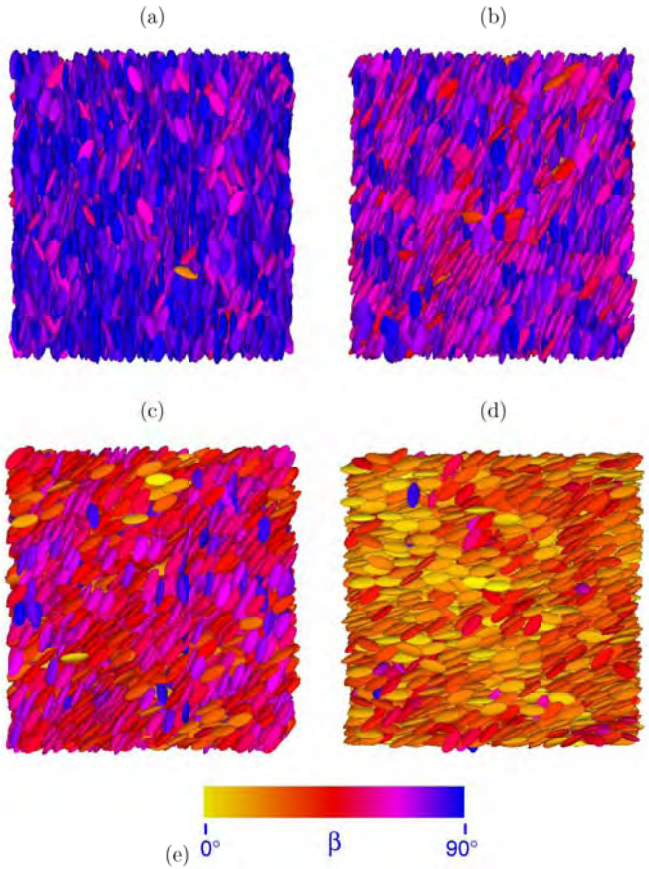

Figure 8